

Deep Deterministic Policy Gradient with Symmetric Data Augmentation for Lateral Attitude Tracking Control of a Fixed-wing Aircraft

Yifei Li, Erik-Jan van Kampen

Abstract

The symmetry of dynamical systems can be exploited for state-transition prediction and to facilitate control policy optimization. This paper leverages system symmetry to develop sample-efficient offline reinforcement learning (RL) approaches. Under the symmetry assumption for a Markov Decision Process (MDP), a symmetric data augmentation method is proposed. The augmented samples are integrated into the dataset of Deep Deterministic Policy Gradient (DDPG) to enhance its coverage of the state-action space. Furthermore, sample utilization efficiency is improved by introducing a second critic trained on the augmented samples, resulting in a dual-critic structure. The aircraft's model is verified to be symmetric, and flight control simulations demonstrate accelerated policy convergence when augmented samples are employed.

Index Terms

reinforcement learning, symmetry, data augmentation, approximate value iteration, flight control.

I. INTRODUCTION

A Common characteristic in the motion of mechanical systems, such as aircraft [1], cars [2] and robotic arms [3], is symmetry, which arises from the symmetric design of their mechanical structures. This characteristic implies that each state trajectory has a symmetric counterpart with respect to a reference plane, and are associated with corresponding symmetric control policies. As a result, the motion of one state trajectory can be leveraged to infer the motion of its symmetric counterpart. An illustrative example is given as the symmetric motions in a cart-pole system [4].

The configurational symmetries of an aircraft frame exhibit two primary types: reflectional and tetragonal symmetries [1]. These structural properties have been exploited to derive conditions under which certain aerodynamic derivatives vanish. They also give rise to kinematic and dynamic symmetries. As a result, aircraft motions exhibit symmetry, which can potentially be leveraged to enhance the learning performance of the RL-based flight control frameworks. In recent years, RL has been successfully applied to flight control design of various aerial vehicles, including quadrotors [5], [6], [7], [8], fixed-wing aircraft [9], [10], [11] and vertical take-off and landing (VTOL) aircraft [12], reducing the dependence on accurate models. In these examples, the flight control law is typically parameterized by a neural network and trained using samples. The quality of a flight dataset, particularly its coverage of the state-action space, directly influences the effectiveness of the learned control law. During the offline training phase, the flight data is generated through the agent interacting with a simulation model, using an exploration policy. However, the convergence of control policy decreases exploration, which may lead to insufficient coverage of the state-action space. This highlights a well-known *exploration and exploitation* trade-off during the learning process [13]. Moreover, inadequate design of the exploration policy can exacerbate this issue by limiting the diversity of collected samples, potentially degrading control performance due to poor generalization of the actor over unvisited regions of the state space. These challenges bring up to the issue of *sample efficiency* during learning. To address this issue, data augmentation techniques have been explored to generate additional training samples based on system properties, such as symmetry [14], [15], [16], [17], [18], [19], [20], [21], [22], leading to *symmetric data augmentation*. A motivation of using symmetric data augmentation for RL-based flight control design is the costly exploration of the high-dimensional state-action space of the aircraft dynamics.

This paper begins by formulating the Q function-based policy optimization method. The symmetry of samples is then defined within an MDP framework. A symmetry condition is derived to determine whether samples are symmetric. This theoretical result motivates a symmetric data augmentation method. Furthermore, the augmented samples are incorporated into the Deep Deterministic Policy Gradient (DDPG) algorithm [23], resulting in a richer dataset. To enhance sample utilization efficiency, we propose a two-step approximate value iteration method. In the first step, the explored samples are used to train a critic and an actor. In the second step, the augmented (symmetric) samples are used to train another critic while updating the same actor. Finally, the symmetry analysis of the aircraft model validates the application of symmetric data augmentation for offline flight control learning.

Yifei Li was with the Section Control and Simulation, Faculty of Aerospace Engineering, Delft University of Technology, Delft, 2629 HS, the Netherlands, e-mail: y.li-34@tudelft.nl.

Erik-Jan van Kampen was with the Section Control and Simulation, Faculty of Aerospace Engineering, Delft University of Technology, Delft, 2629 HS, the Netherlands, e-mail: e.vankampen@tudelft.nl.

Manuscript received September 12, 2025; revised October 26, 2025.

The main contributions of this paper are summarized as:

- A symmetric data augmentation method is proposed to generate additional training samples.
- A two-step approximate policy iteration method is developed to enhance sample utilization efficiency during training.
- The symmetry of the aircraft's model is analyzed, and symmetry-informed RL frameworks are applied for learning flight control laws.

This paper is structured as follows. Section II formulates the discrete-time optimal control problem and the approximate value iteration method. Section III defines the symmetry characteristics of a dynamical system. Section IV introduces the symmetric data augmentation method. Section V develops the DDPG with symmetric critic augmentation. Section VI presents the aircraft dynamical model and analyzes its symmetry. Section VII introduces action smoothness techniques. Section VIII provides simulation results of symmetry-informed RL for flight control. Section IX concludes this paper.

A. Related Work

1) *Symmetric data augmentation for RL*: Symmetric data augmentation relies on the assumption of symmetry throughout the state-action space. This assumption implies that each state trajectory has a symmetric counterpart, allowing samples from an explored trajectory to be used to generate samples from its symmetric counterpart, without further interaction with the environment. This method increases the number of training samples, thereby improving sample efficiency, which is an especially important advantage when applying RL to complex, high-dimensional systems where exploration of the state-action space is costly. In [14], the explored samples are mirrored according to a simple symmetric relation and incorporated into maximum a posterior policy optimization to accelerate learning. In [15], [16], an expert-guided detection method is developed to verify symmetry by assuming system dynamics are invariant. The detected symmetry is used to augment samples to learn the transition functions of Grid, Cart-pole and Acrobot systems. In [17], the Lie point symmetry group is used to augment samples for solving a neural partial differential equation (PDE). In [18], [19], the generalization bounds for data augmentation method is theoretically analyzed using symmetry. In [20], [21], symmetric data augmentation is combined with experience replay techniques, leading to Kaleidoscope Experience Replay based on reflectional symmetry, and Goal-augmented Experience Replay, a direct generalization of Hindsight Experience Replay. Reference [22] learns the equivariance set of an MDP and uses it for data augmentation in offline RL. Reference [24] employs a pre-trained forward model for Koopman latent representation of equivariant dynamical systems, enabling symmetric data augmentation for Q -learning.

2) *DDPG/TD3 for flight control*: DDPG and twin-delayed DDPG (TD3) are deterministic, off-policy reinforcement learning approaches, enabling policy optimization through a state-action (Q) value function over the continuous state-action space of aircraft dynamics. In flight control designs, these methods reduce reliance on accurate system models by leveraging samples and thus mitigate the challenges associated with modeling aerodynamic coefficients, actuator dynamics, and other unknown dynamics. Comprehensive surveys of related research can be found in [25], [26]. Specific applications include attitude control design for the Flying-V [27], Cessna Citation PH-LAB [28], quadrotors [29], [30], [31], [32], [33], [5], [34], [35], the F-16 model [36], jetstream [37], fixed-wing UAV [38], [39], [40], UAV automatic carrier landing system [41], the Internet-of-Drones [33], Skyhunter [42], monocopter [43], flying-wing aircraft [44].

II. FOUNDATIONS

This section formulates an infinite-horizon optimal control problem. First, the state-value (V) function and the state-action value (Q) function are defined to evaluate the values of states and actions. Next, the numerical solution methods, namely, exact value iteration and approximate value iteration, are introduced.

A. Definitions

Consider a discrete-time control-affine nonlinear system as

$$x_{t+1} = F(x_t)x_t + G(x_t)u_t, t \in \mathbb{N} \quad (1)$$

where $x_t \in \mathbb{R}^n$ is the state vector, $u_t \in \mathbb{R}^m$ is the input vector. $F(x_t) \in \mathbb{R}^{n \times n}$, $G(x_t) \in \mathbb{R}^{n \times m}$ are nonlinear functions associated with the state vector x_t . The subscript t denotes the index of the time step. \mathbb{N} represents the set of non-negative integers.

Define a performance index starting from an initial state x_0 as

$$J(x_0, u_0) = \sum_{t=0}^{\infty} \gamma^t r(x_t, u_t) \quad (2)$$

where $r(x_t, u_t)$ is a reward function defined at timestep t . $\gamma \in [0, 1]$ is the discount factor. The control action series u_t ($t = 0, 1, 2, \dots$) is generated by a state-feedback control $u_t = h(x_t)$.

Assumption 1. The policy $h(x)$ is a Lipschitz continuous function of state x .

This assumption can be satisfied in the control design of real-world mechanical systems. This condition ensures the existence of the policy gradient, which facilitates gradient-based policy search. A policy represented by a neural network can satisfy this condition by using Lipschitz-continuous activation functions, such as tanh, ReLu [45], [46], [47].

Definition 1. The state-value function $V^h : \mathbb{R}^n \rightarrow \mathbb{R}_+$, which starts from any initial state x_0 and follows a policy $h(\cdot)$, is defined by

$$V^h(x_0) = \sum_{t=0}^{\infty} \gamma^t r(x_t^h, h(x_t^h)) \quad (3)$$

where x_t^h denotes the state x_t following a control policy $h(\cdot)$.

Definition 2. The state action-value function $Q^h : \mathbb{R}^{n+m} \rightarrow \mathbb{R}_+$, which starts from any initial state x_0 and takes an action a_0 , then follows a policy $h(\cdot)$, is defined by

$$Q^h(x_0, a_0) = r(x_0, a_0) + \sum_{t=1}^{\infty} \gamma^t r(x_t^h, h(x_t^h)) \quad (4)$$

Rewrite Equation 3 in a recursive form as

$$V^h(x_0) = r(x_0, u_0) + \gamma V^h(x_1) \quad (5)$$

which is known as the Bellman equation for $V^h(x_0)$ [13].

Rewrite Equation 4 in a recursive form as

$$Q^h(x_0, a_0) = r(x_0, a_0) + \gamma V^h(x_1) \quad (6)$$

which is known as the Bellman equation for $Q^h(x_0, a_0)$.

B. Policy optimization based on Q function

For a deterministic control policy $h(\cdot)$, by setting $a_0 = h(x_0)$, the following equation holds:

$$V^h(x_0) = Q^h(x_0, h(x_0)) \quad (7)$$

Substituting 7 into 6:

$$Q^h(x_0, a_0) = r(x_0, a_0) + \gamma Q^h(x_1, h(x_1)) \quad (8)$$

Denote an optimal policy that maximizes the state-value function $V^h(x_0)$ with $u_t^* = h^*(x_t)$ ($t = 0, 1, 2, \dots$), defined by:

$$h^*(x_0) \in \arg \max_{h(\cdot)} V^h(x_0) \quad (9)$$

Substitute 9 into 5:

$$V^{h^*}(x_0) = \max_{h(x_0)} [r(x_0, u_0) + \gamma V^h(x_1)] \quad (10)$$

Denote an optimal control policy that maximizes $V^h(x_{t+1})$ with $u^*(x_{t+1}) = h^*(x_{t+1})$ ($t = 0, 1, 2, \dots$), defined by:

$$h^*(x_{t+1}) \in \arg \max_{h(\cdot)} V^h(x_{t+1}) \quad (11)$$

In addition, the optimal Q function associated with state x_0 and action a_0 is defined by

$$\begin{aligned} [Q^h(x_0, a_0)]^* &:= Q^{h^*}(x_0, a_0) \\ &= \max_{h(\cdot)} [r(x_0, a_0) + \gamma V^h(x_1)] \\ &= r(x_0, a_0) + \gamma V^{h^*}(x_1) \end{aligned} \quad (12)$$

which is understood as a result of taking action a_0 at x_0 and following an optimal control policy $u_{t+1}^* = h^*(x_{t+1})$.

The optimal action a_0^* is defined to be the action that maximizes $Q^h(x_0, a_0)$:

$$\begin{aligned}
a_0^* &\in \arg \max_{a_0} [Q^h(x_0, a_0)] \\
&= \arg \max_{a_0} [r(x_0, a_0) + \gamma V^h(x_1)] \\
&= \arg \max_{a_0} [r(x_0, a_0) + \gamma Q^h(x_1, h(x_1))]
\end{aligned} \tag{13}$$

Substitute 13 into Equation 6:

$$Q^h(x_0, a_0^*) = \max_{a_0} (r(x_0, a_0) + \gamma Q^h(x_1, h(x_1))) \tag{14}$$

C. Exact value iteration

To solve the optimal action a_0^* in Equation 14, the exact value iteration method [13] is introduced that is able to iteratively evaluate and improve a current action $a_0 = h(x_0)$ as follows.

Policy Evaluation

$$(Q^h)^{i+1}(x_t, a_t) = r(x_t, a_t) + \gamma (Q^h)^i(x_{t+1}, h(x_{t+1})) \tag{15}$$

Policy Improvement

$$h^{i+1}(x_t) = \arg \max_{h(\cdot)} ((Q^h)^{i+1}(x_t, h(x_t))) \tag{16}$$

where the index i denotes the i -th iteration of policy evaluation and policy improvement.

D. Approximate value iteration

Practically, the structures of functions $Q^h(x_t, a_t), h(x_t)$ are usually unknown, making it difficult to solve Equations 15, 16. These functions can be parameterized using neural networks, which enables an approximate approach to solve these equations, namely Approximate Value iteration (AVI) [48]. AVI uses two neural networks: (1) the critic network approximates the state-action value function and is denoted as $\hat{Q}_\psi^h(x_t, a_t)$, with a parameter set ψ ; (2) The actor network approximates the policy $h(x_t)$ and is denoted as $\mu_\vartheta(x_t)$, with a parameter set ϑ . Therefore, Equations 15, 16 can be reconstructed as

Approximate Policy Evaluation

$$(\hat{Q}_\psi^h)^{i+1}(x_t, a_t) = r(x_t, a_t) + \gamma (\hat{Q}_\psi^h)^i(x_{t+1}, (\mu_\vartheta)^i(x_{t+1})) \tag{17}$$

Approximate Policy Improvement

$$(\mu_\vartheta)^{i+1}(x_t) = \arg \max_{\vartheta} [(\hat{Q}_\psi^h)^{i+1}(x_t, \mu_\vartheta(x_t))] \tag{18}$$

The parameter sets ψ, ϑ are numerically obtained from the above equations using the gradient descent method within the DDPG framework.

III. SYMMETRIC DYNAMICAL MODEL

The Markov property of system 1 is assumed to hold and is defined as: the transition of states depends merely on the present states and actions, and not on any previous states [13]. Accordingly, a sample of state transition is represented as (x_t, a_t, x_{t+1}) , indicating that the system transitions from x_t to x_{t+1} when action a_t is applied.

Definition 3. (Symmetric one-step state transitions) Two state transition samples (x_t, a_t, x_{t+1}) and (x'_t, a'_t, x'_{t+1}) are symmetric to a reference state x^* if

$$\frac{x_t + x'_t}{2} = x^* \tag{19}$$

$$a_t = -a'_t \tag{20}$$

$$\frac{x_{t+1} + x'_{t+1}}{2} = x^* \tag{21}$$

Assuming Equations 19, 20 hold, the following theorem discusses the condition under which Equation 21 holds.

Theorem 1. (Symmetry of x_{t+1}) Select two samples from the system 1, denoted as (x_t, a_t, x_{t+1}) , (x'_t, a'_t, x'_{t+1}) , and a reference state $x = x^*$. Assuming Equations 19, 20 hold, then x_{t+1}, x'_{t+1} are symmetric with respect to x^* when

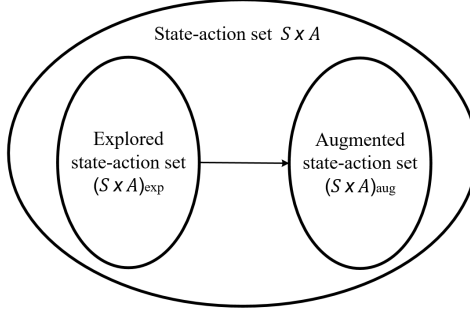


Fig. 1: A sketch map of symmetry in state-action set $\mathcal{S} \times \mathcal{A}$ of a dynamical system. The whole state-action set $\mathcal{S} \times \mathcal{A}$ contains two subsets: (1) state-action set of explored samples, denoted as $(\mathcal{S} \times \mathcal{A})_{\text{exp}}$; (2) state-action set of augmented samples, denoted as $(\mathcal{S} \times \mathcal{A})_{\text{aug}}$

- (1) $x^* = 0 \in \mathbb{R}^n, G(x_t) = G(x'_t), F(x_t) = F(x'_t)$
- (2) $x^* \neq 0 \in \mathbb{R}^n, G(x_t) = G(x'_t), F(x_t) = F(x'_t) = I \in \mathbb{R}^{n \times n}$.

Proof. See Appendix □

Definition 4. The system 1 is a symmetric dynamical system with respect to a reference state x^* if

$$\begin{aligned} \frac{x_t + x'_t}{2} &= x^*, \quad \forall x_t, x'_{t+1} \in \mathcal{S} \\ a_t &= -a'_t, \quad \forall a_t, a'_{t+1} \in \mathcal{A} \\ \frac{x'_{t+1} + x'_{t+2}}{2} &= x^*, \quad \forall x'_t, x'_{t+1} \in \mathcal{S} \end{aligned} \quad (22)$$

where $\mathcal{S} \in \mathbb{R}^n, \mathcal{A} \in \mathbb{R}^m$ denote the state and the action spaces. This symmetry relation is illustrated in Figure 1.

Definition 5. The reward function $r(x_t, a_t)$ is symmetric at state-action pairs (x_t, a_t) and (x'_t, a'_t) if

$$r(x_t, a_t) = r(x'_t, a'_t) \quad (23)$$

Definition 6. The action-value function $Q^h(x_t, a_t)$ in Equation 4 is symmetric at state-action pairs (x_k, a_t) and (x'_t, a'_t) if

$$Q^h(x_t, a_t) = Q^h(x'_t, a'_t) \quad (24)$$

IV. DDPG WITH SYMMETRIC DATA AUGMENTATION

This section develops a symmetric data augmentation method based on assumptions made in Section III. The augmented samples are used in the framework of DDPG to improve sample efficiency.

A. Symmetric data augmentation

According to Equations 19, 20, 21, 23, The augmented samples can be obtained by mirroring the explored samples as

$$s'_t = As_t + Bx^* \quad (25)$$

where $s_t = [x_t, a_t, x_{t+1}, r_t]^T$ is an explored sample, $s'_t = [x'_t, a'_t, x'_{t+1}, r'_t]^T$ is an augmented sample. The matrices A and B are defined as

$$A = \begin{bmatrix} -1 & 0 & 0 & 0 \\ 0 & -1 & 0 & 0 \\ 0 & 0 & -1 & 0 \\ 0 & 0 & 0 & -1 \end{bmatrix}, B = \begin{bmatrix} 2 \\ 0 \\ 2 \\ 0 \end{bmatrix} \quad (26)$$

B. DDPG with symmetric data augmentation

DDPG is a Q -learning-based approach that uses mini-batch learning. The critic is trained to approximate the Q -function, while the actor is trained to approximate the optimal policy [23]. This can be implemented through approximate value iteration (AVI). A replay buffer \mathcal{D} is used to store collected samples and the augmented samples as

$$s_t \in \mathcal{D}, s'_t \in \mathcal{D} \quad (27)$$

In this way, the dataset is enriched. A mini-batch consisting of both explored and augmented samples can be selected to train the critic and actor. This leads to an improved DDPG algorithm that exploits the augmented samples, namely the Deep Deterministic Policy Gradient with Symmetric Data Augmentation (DDPG-SDA). A brief flowchart is shown in Figure 2 (left). The pseudocode code is provided in Algorithm V-D.

V. DDPG WITH SYMMETRIC CRITIC AUGMENTATION

This section investigates how to improve the sample utilization efficiency of DDPG-SDA. We show that using mixed samples within a batch is not effective for fully exploiting the augmented samples. Based on this analysis, we propose two modifications to the algorithmic structure: (1) Q -function approximation with two critic networks; (2) the two-step approximate value iteration.

A. Drawback of DDPG-SDA

Mixing explored and augmented samples within a mini-batch may not significantly improve the convergence of a policy, as the number of explored samples is reduced compared to a mini-batch containing only explored data. One possible solution to this issue is to increase the mini-batch size, but this may conversely degrade learning performance [49]. Therefore, it is worthwhile to investigate ways to improve policy convergence without changing the mini-batch size.

B. Dual critics for Q function approximation

To exploit the augmented dataset more efficiently, we propose separate storage and sampling of explored and augmented samples. To this end, two replay buffers, denoted by \mathcal{D}_1 and \mathcal{D}_2 , are used to store the explored and augmented samples separately:

$$s_t \in \mathcal{D}_1, s'_t \in \mathcal{D}_2 \quad (28)$$

As such, the two types of samples can be sampled separately and used to train two critics. Consequently, the approximation of the Q -function is through:

$$Q^h(x_t, a_t) \approx \begin{cases} \hat{Q}_{\psi_1}^h(x_t, a_t), & \text{if } (x_t, a_t) \in \mathcal{D}_1 \\ \hat{Q}_{\psi_2}^h(x_t, a_t), & \text{if } (x_t, a_t) \in \mathcal{D}_2 \end{cases} \quad (29)$$

where ψ_1, ψ_2 are parameter sets of the two critics.

C. Two-step approximate value iteration

The two critics and the actor are trained based on a two-step approximate value iteration method:

Step 1 (AVI on a mini-batch from \mathcal{D}_1):

$$(\hat{Q}_{\psi_1}^h)^{i+1}(x_t, a_t) = r(x_t, a_t) + \gamma(\hat{Q}_{\psi_1}^h)^i(x_{t+1}, (\mu_\vartheta)^i(x_{t+1})) \quad (30)$$

$$(\mu_\vartheta)^{i+1}(x_t) = \arg \min_{\vartheta} \left[(\hat{Q}_{\psi_1}^h)^{i+1}(x_t, \mu_\vartheta(x_t)) \right] \quad (31)$$

Step 2 (AVI on a mini-batch from \mathcal{D}_2):

$$(\hat{Q}_{\psi_2}^h)^{i+1}(x_t, a_t) = r(x_t, a_t) + \gamma(\hat{Q}_{\psi_2}^h)^i(x_{t+1}, (\mu_\vartheta)^{i+1}(x_{t+1})) \quad (32)$$

$$(\mu_\vartheta)^{i+2}(x_t) = \arg \min_{\vartheta} \left[(\hat{Q}_{\psi_2}^h)^{i+1}(x_t, \mu_\vartheta(x_t)) \right] \quad (33)$$

Remark 1. Step 1 trains the critic and actor networks on a mini-batch of samples from \mathcal{D}_1 , while Step 2 trains them again on a mini-batch from \mathcal{D}_2 . As a result, the critic networks are trained separately with explored and augmented samples, whereas the actor is trained on samples from both datasets. The corresponding parameter update equations are provided in the Appendix.

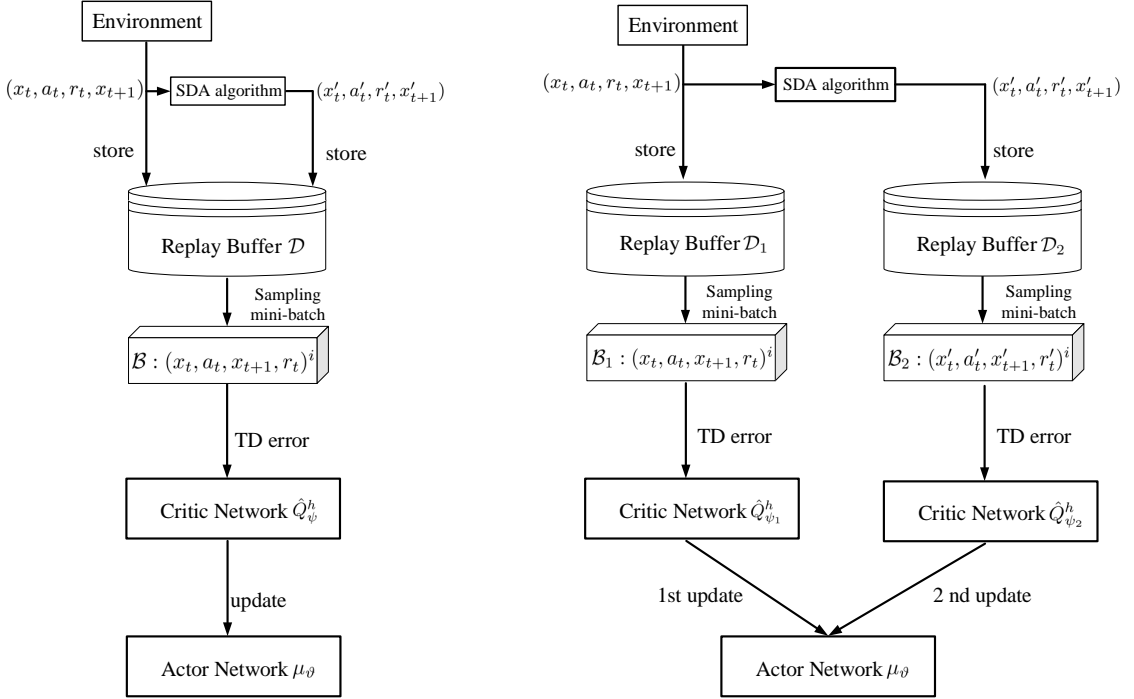


Fig. 2: Brief flowcharts of DDPG-SDA (left) and DDPG-SCA (right). Both methods employ symmetric data augmentation to generate additional samples. DDPG-SDA stores both types of samples in a single replay buffer, whereas DDPG-SCA stores them separately in two replay buffers and adopts a dual-critic structure to enable separate training with explored and augmented samples.

Algorithm 1: DDPG-SDA Algorithm

1: Hyperparameters: Critic/actor learning rates $\eta_{\text{critic}}, \eta_{\text{actor}}$, mini-batch size N , delay factor τ , discount factor γ , maximal environment step t_{\max} , maximal episode number N_{eps} , Ornstein–Uhlenbeck process parameters σ, θ, dt [50]
2: Initialization: Critic network parameter set ψ , actor network parameter set ϑ , empty replay buffer \mathcal{D} , target critic network parameter set $\psi_{\text{target}} \leftarrow \psi$, target actor network parameter set $\vartheta_{\text{target}} \leftarrow \vartheta$
4: **for** episode $\leftarrow 1$ to N_{eps} **do**
5: **for** environment step $t \rightarrow 0$ to t_{\max} **do**
6: Observe state x_t and select action
 $a_t = \mu_\vartheta(x_t) + \epsilon, \epsilon \sim \text{OU}(\sigma, \theta, dt)$
7: Execute a_t in the environment
8: Observe next state x_{t+1} , reward r_t , and done signal d_t that indicates whether x_{t+1} is terminal
9: Store sample $s_t = (x_t, a_t, r_t, x_{t+1})$ and d_t in replay buffer \mathcal{D}
9: Calculate symmetric sample s'_t using

$$s'_t = A s_t + B x^*$$

10: Store sample $s'_t = (x'_t, a'_t, r'_t, x'_{t+1})$ and $d'_t = d_t$ in replay buffer \mathcal{D}
11: **If** x_{t+1} is terminal **then**
12: reset environment state
13: **If** training is true **then**
14: **for** each update step **do**
15: Randomly choose N samples from \mathcal{D} to compose sample set \mathcal{B}

$$\mathcal{B} = \{(x_t, a_t, r_t, x_{t+1}, d_t)^i | i=1, 2, \dots, N\}$$

16: Calculate target values of samples in \mathcal{B} with

$$z^i = r_t^i + \gamma(1 - d_t^i) \hat{Q}_{\psi_{\text{target}}}^h[x_{t+1}^i, \mu_{\vartheta_{\text{target}}}(x_{t+1}^i)]$$

17: Update parameter set ψ for one step using gradient:

$$\nabla_\psi \frac{1}{N} \sum_{i=1}^N [\hat{Q}_\psi^h(x_t^i, a_t^i) - z^i]^2$$

18: Update parameter set ϑ for one step using gradient:

$$\nabla_\vartheta \frac{1}{N} \sum_{i=1}^N \hat{Q}_\psi^h[x_t^i, \mu_\vartheta(x_t^i)]$$

19: Update parameter sets $\psi_{\text{target}}, \vartheta_{\text{target}}$ with

$$\psi_{\text{target}} \leftarrow \tau \psi_{\text{target}} + (1 - \tau) \psi$$

$$\vartheta_{\text{target}} \leftarrow \tau \vartheta_{\text{target}} + (1 - \tau) \vartheta$$

20: **end for**
21: **end if**
22: **until** convergence

Algorithm 2: DDPG-SCA Algorithm

1: Hyperparameters: critic/actor learning rate $\eta_{\text{critic}}, \eta_{\text{actor}}$, delay factor τ
 mini-batch size N , update step N_{update} , discount factor γ
 Ornstein–Uhlenbeck (OU) process [50] parameters σ, θ, dt

2: Initialization: critic network parameter sets ψ_1, ψ_2 , actor network
 parameter set ϑ , empty replay buffers $\mathcal{D}_1, \mathcal{D}_2$

3: Initialization: target critic network parameter sets $\psi_{1\text{target}} \leftarrow \psi_1$,
 $\psi_{2\text{target}} \leftarrow \psi_2$
 target actor network parameter sets $\vartheta_{\text{target}} \leftarrow \vartheta$

4: **Repeat**

5: Observe state x_t and select action
 $a_t = \mu_\vartheta(x_t) + \epsilon, \epsilon \sim \text{OU}(\sigma, \theta, dt)$

6: Execute a_t in the environment

7: Observe next state x_{t+1} , reward r_t , and done signal d_t that indicates
 whether x_{t+1} is terminal

8: Store sample $s_t = (x_t, a_t, r_t, x_{t+1})$ and d_t in replay buffer \mathcal{D}_1

9: Calculate symmetric sample s'_t using
 $s'_t = A s_t + B x^*$

10: Store sample $s'_t = (x'_t, a'_t, r'_t, x'_{t+1})$ and $d'_t = d_t$ in replay buffer \mathcal{D}_2

11: **If** x_{t+1} is terminal **then**

12: reset environment state

13: **If** training is true **then**

14: **for** each update step **do**

15: Randomly choose n samples from \mathcal{D}_1 to compose sample set \mathcal{B}_1
 $\mathcal{B}_1 = \{(x_t, a_t, r_t, x_{t+1}, d_t)^i | i=1, 2, \dots, N\}$

16: Calculate target values of samples in \mathcal{B}_1 with
 $z^i = r_t^i + \gamma(1 - d_t^i) \hat{Q}_{\psi_{1\text{target}}}^h[x_{t+1}^i, \mu_{\vartheta_{1\text{target}}}(x_{t+1}^i)]$

17: Update parameter set ψ_1 for one step using gradient:
 $\nabla_{\psi_1} \frac{1}{N} \sum_{i=1}^N [\hat{Q}_{\psi_1}^h(x_t^i, a_t^i) - z^i]^2$

18: Update parameter set ϑ for one step using gradient:
 $\nabla_{\vartheta} \frac{1}{N} \sum_{i=1}^N \hat{Q}_{\psi_1}^h[x_t^i, \mu_\vartheta(x_t^i)]$

19: Update parameter sets $\psi_{1\text{target}}, \vartheta_{\text{target}}$ with
 $\psi_{1\text{target}} \leftarrow \tau \psi_{1\text{target}} + (1 - \tau) \psi_1$
 $\vartheta_{\text{target}} \leftarrow \tau \vartheta_{\text{target}} + (1 - \tau) \vartheta$

20: Randomly choose n samples from \mathcal{D}_2 to compose sample set \mathcal{B}_2
 $\mathcal{B}_2 = \{(x_t, a_t, r_t, x_{t+1}, d_t)^i | i=1, 2, \dots, N\}$

21: Calculate target values of samples in \mathcal{B}_2 with
 $z^i = r_t^i + \gamma(1 - d_t^i) \hat{Q}_{\psi_{2\text{target}}}^h[x_{t+1}^i, \mu_{\vartheta_{\text{target}}}(x_{t+1}^i)]$

22: Update parameter set ψ_2 for one step using gradient:
 $\nabla_{\psi_2} \frac{1}{N} \sum_{i=1}^N [\hat{Q}_{\psi_2}^h(x_t^i, a_t^i) - z^i]^2$

23: Update parameter set ϑ for one step using gradient:
 $\nabla_{\vartheta} \frac{1}{N} \sum_{i=1}^N \hat{Q}_{\psi_2}^h[x_t^i, \mu_\vartheta(x_t^i)]$

24: Update parameter sets $\psi_{2\text{target}}, \vartheta_{\text{target}}$ with
 $\psi_{2\text{target}} \leftarrow \tau \psi_{2\text{target}} + (1 - \tau) \psi_2$
 $\vartheta_{\text{target}} \leftarrow \tau \vartheta_{\text{target}} + (1 - \tau) \vartheta$

25: **end for**

26: **end if**

27: **until** convergence

D. DDPG with symmetric critic augmentation

The proposed modifications make DDPG with symmetric critic augmentation (SCA). The advantage lies in the more effective utilization of augmented samples without increasing the mini-batch size, which can potentially lead to faster policy convergence during learning (as demonstrated in the simulation results). A brief flowchart is shown in Figure 2 (right). The pseudocode is seen in Algorithm V-D.

VI. MODEL

This subsection introduces the aircraft lateral dynamics. First, a continuous-time linear model is introduced. Next, this model is discretized using the Euler method. Finally, the symmetry of discrete-time model is analyzed based on Theorem 1.

A. Aircraft model

1) *Dynamical model:* The aircraft dynamical model is described by the differential equations [51]:

$$\begin{aligned} \dot{\phi} &= p \\ \dot{p} &= L'_p p + L'_r r + L'_\beta \beta + L'_{\delta_a} \delta_a + L'_{\delta_r} \delta_r \\ \dot{\beta} &= Y_p^* p + Y_\phi^* \phi + (Y_r^* - 1) r + Y_\beta \beta + Y_{\delta_a}^* \delta_a + Y_{\delta_r}^* \delta_r \\ \dot{r} &= N'_p p + N'_r r + N'_\beta \beta + N'_{\delta_a} \delta_a + N'_{\delta_r} \delta_r \end{aligned} \tag{34}$$

where ϕ is bank angle, p is roll rate, β is sideslip angle, r is yaw rate. δ_a is the aileron deflection, δ_r is the rudder deflection. Aerodynamic coefficients are seen in Table I.

2) *Discretization:* The differential equations 34 can be discretized using the Euler's method [52] with a time step Δt :

$$\begin{aligned}\phi_{t+1} &= \phi_t + p_t \Delta t \\ p_{t+1} &= p_t + (L'_p p_t + L'_r r_t + L'_\beta \beta_t + L'_{\delta_a} \delta_{a(t)} + L'_{\delta_r} \delta_{r(t)}) \Delta t \\ \beta_{t+1} &= \beta_t + [Y_p^* p_t + Y_\phi^* \phi_t + (Y_r^* - 1) r_t + Y_\beta \beta_t + Y_{\delta_a}^* \delta_{a(t)} + Y_{\delta_r}^* \delta_{r(t)}] \Delta t \\ r_{t+1} &= r_t + [N'_p p_t + N'_r r_t + N'_\beta \beta_t + N'_{\delta_a} \delta_{a(t)} + N'_{\delta_r} \delta_{r(t)}] \Delta t\end{aligned}\quad (35)$$

Rewrite equations 35 as

$$x_{t+1} = F(x_t)x_t + G(x_t)u_t \quad (36)$$

where $x_t = [\phi_t, p_t, \beta_t, r_t]^T$, $u_t = [\delta_{a(t)}, \delta_{r(t)}]^T$, and $F(x_t), G(x_t)$ are given by

$$F(x_t) = \begin{bmatrix} 1 & T & 0 & 0 \\ 0 & 1 + L'_p \Delta t & L'_\beta \Delta t & L'_r \Delta t \\ Y_\phi^* \Delta t & Y_p^* \Delta t & 1 + Y_\beta \Delta t & (Y_r^* - 1) \Delta t \\ 0 & N'_p \Delta t & N'_\beta \Delta t & (1 + N'_r \Delta t) \end{bmatrix}, G(x_t) = \begin{bmatrix} 0 & 0 \\ L'_{\delta_a} \Delta t & L'_{\delta_r} \Delta t \\ Y_{\delta_a}^* \delta_{a(t)} \Delta t & Y_{\delta_r}^* \Delta t \\ N'_{\delta_a} \delta_{a(t)} \Delta t & N'_{\delta_r} \delta_{r(t)} \Delta t \end{bmatrix} \quad (37)$$

B. Symmetry analysis

This subsection analyzes the symmetry of the aircraft lateral dynamics described by Equations 36. Theorem 1 classifies symmetry planes into two cases: $x^* = 0$ and $x^* \neq 0$. The latter case requires a stricter constraint on the system matrix $F(x_t)$. Equations 35 also exhibit coupling effects among state increments from time step t to $t+1$, which are captured in $F(x_t)$. The coupling effects would influence symmetry of the overall system.

Apply the assumptions of Theorem 1 to system 36:

$$\begin{aligned}\frac{x_t + x'_t}{2} &= x^* \\ a_t &= -a'_t\end{aligned}\quad (38)$$

where $x_t = [\phi_t, p_t, \beta_t, r_t]$, $x'_t = [\phi'_t, p'_t, \beta'_t, r'_t]$ are state pairs symmetric about the reference plane $x^* = [\phi^*, p^*, \beta^*, r^*]$, $a_t = [\delta_{a(t)}, \delta_{r(t)}]$, $a'_t = [\delta'_{a(t)}, \delta'_{r(t)}]$ are action pairs symmetric about $0 \in \mathbb{R}^n$.

Because conditions $F(x_k) = F(x'_k) \neq 0 \in \mathbb{R}^{n \times n}$, $G(x_k) = G(x'_k)$ hold for system 36, one can conclude from case (1) of Theorem 1 that

$$\frac{x_{t+1} + x'_{t+1}}{2} = 0 \in \mathbb{R}^n \quad (39)$$

where $x_{t+1} = [\phi_{t+1}, p_{t+1}, \beta_{t+1}, r_{t+1}]$, $x'_{t+1} = [\phi'_{t+1}, p'_{t+1}, \beta'_{t+1}, r'_{t+1}]$.

TABLE I: Aerodynamic coefficients (adopted from [51])

Parameter	Value	Parameter	Value
L'_p	-1.699	Y_p^*	0
L'_r	0.172	Y_ϕ^*	0.0488
L'_β	-4.546	Y_r^*	0
N'_p	-0.0654	Y_β	-0.0829
N'_r	-0.0893	L'_{δ_a}	27.276
N'_β	3.382	L'_{δ_r}	0.576
$Y_{\delta_a}^*$	0	$Y_{\delta_r}^*$	0.116
N_{δ_a}	0.395	N_{δ_r}	-1.362

VII. CONDITIONING FOR ACTION POLICY SMOOTHNESS

Conditioning for Action Policy Smoothness (CAPS) techniques have been developed to achieve smooth control of a quadrotor in offline RL frameworks [32], and adapted for smooth control of the Flying-V and Cessna Citation PH-LAB aircraft [28], [53], [54], [55]. The core idea is to incorporate smoothness losses into policy optimization, which can be viewed as a multiple-objective optimization problem that explicitly considers action smoothness. This approach encourages the actor to produce similar actions for neighboring input states that vary across spatial or temporal scales.

For a mini-batch, the spatial smoothness loss can be formulated as

$$L_s = \frac{1}{n_s} \sum_{j=1}^n \left\| \mu_\vartheta(\bar{x}_t^j) - \mu_\vartheta(x_t^j) \right\|_2 \quad (j = 1, 2, \dots, n_s) \quad (40)$$

where x_t is the input of the actor at time step t , \bar{x}_t is the biased x_t in spatial scale, j is the index of n_s biased states sampled from the distribution of measured x_t . The spatial smoothness loss penalizes the changes of actions with respect to the state biases caused by measurement noises, which is helpful to improve generalization and robustness of the policy.

For a mini-batch, the temporal smoothness loss can be formulated as

$$L_t = \frac{1}{n} \sum_{i=1}^n \left\| \mu_\vartheta(x_{t+1}^i) - \mu_\vartheta(x_t^i) \right\|_2 \quad (i = 1, 2, \dots, n) \quad (41)$$

where x_{t+1}, x_t are the input of the actor at time steps t and $t+1$, i is the index of n samples in a mini-batch.

The temporal smoothness loss measures changes in the actor's output in response to changes in the input in temporal scale. The abrupt variations in actions between consecutive time steps are penalized so that the actor learns to produce a series of slow-varying actions over time.

A multi-objective optimization is then formulated as

$$h(x_t^i) = \arg \max_h \left(\sum_{i=1}^n \left[\hat{Q}_\psi^h(x_t^i, h(x_t^i)) \right] - \lambda_1 L_s - \lambda_2 L_t \right) \quad (42)$$

where the first term measures long-term state-action values and $\lambda_1 \geq 0, \lambda_2 \geq 0$ are weights of the smoothness losses. These parameters can be tuned to balance the state-action value estimation and the smoothness of the actions.

VIII. SIMULATION

This section presents the flight control simulation results. The symmetry-informed RL algorithms are evaluated during both the online training and online operation phases. Furthermore, the generalization capability of the trained actors is assessed by tracking a bank-angle reference that was not used during policy training.

A. Environment settings

The environment is set as the aircraft model described in Equations 34. These differential equations are integrated using the fourth-order Runge–Kutta method with a time step of 0.01s. Each episode consists of 300 time steps. The weights of the critic, actor, and their corresponding target networks are initialized using the Kaiming distribution [56] provided by PyTorch's linear module. Sampling from replay buffers is performed without replacement, to ensure the full diversity of the samples in a mini-batch, improving sample efficiency in each update of networks. The aircraft state vector $[\phi, p, \beta, r]^T$ is initialized randomly by uniform distributions, i.e. $\phi_0 \sim U(0^\circ, 20^\circ)$, $p_0 \sim U(0^\circ/\text{s}, 10^\circ/\text{s})$, $\beta_0 \sim U(0^\circ, 20^\circ)$, $r_0 \sim U(0^\circ/\text{s}, 10^\circ/\text{s})$. Actuator actions are constrained as $\delta_a, \delta_r \in [-57.3^\circ, 57.3^\circ]$, which defines an action space $\mathcal{A} = [-57.3^\circ, 57.3^\circ] \times [-57.3^\circ, 57.3^\circ] \in \mathbb{R}^2$. The bank angle reference ϕ_{ref} is set as a square-wave signal with a period of $T = 3$ s. The amplitude A is selected at the beginning of each episode by sampling it from a uniform distribution $U(0^\circ, 30^\circ)$. The environment state is augmented with tracking error as $[e_\phi, \phi, p, \beta, r]^T \in \mathbb{R}^5$, where $e_\phi = \phi - \phi_{\text{ref}}$. The reward function is shaped to promote bank angle tracking and sideslip angle stabilization, i.e. $\phi \rightarrow \phi_{\text{ref}}, \beta \rightarrow 0$. The aggressive control behaviors are constrained by penalizes excessive angular rates and control efforts. The reward function is given as

$$r_t = -10 \|\text{clip}(5e_t, -1, 1)\|_1 - \|p_t\|_1 - \|r_t\|_1 - 0.01\|\delta_{a(t)}\|_1 - 0.01\|\delta_{r(t)}\|_1 \quad (43)$$

where tracking error vector is defined as $e_t = [e_{\phi_t}, e_{\beta_t}]^T \in \mathbb{R}^{2 \times 1}$, $e_{\phi_t} = \phi_t - \phi_{\text{ref}(t)}$, $e_{\beta_t} = \beta_t - 0$. The function $\text{clip}(\cdot)$ is used to amplify tracking errors e_{ϕ_t} in the set $\{e_{\phi_t} | 0.2 < |e_{\phi_t}| < 1\}$, and e_{β_t} in the set $\{e_{\beta_t} | 0.2 < |e_{\beta_t}| < 1\}$. $\|\cdot\|_1$ is the 1-norm operator. Figure 4 illustrates the overall architecture of the RL-based flight control system.

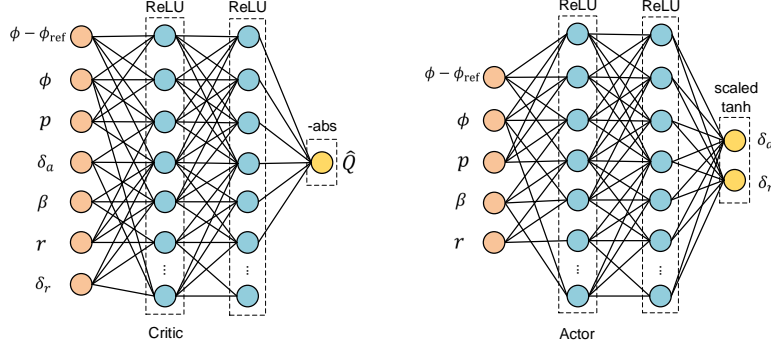


Fig. 3: The network architectures of the critic and actor. The critic takes all the states, actions and the tracking error of bank angle as input, and outputs the estimated state-action values, with a $-\text{abs}(\cdot)$ activation function applied at the output layer to ensure the negative definiteness of the estimated state-action value function. The actor outputs the control surface deflections δ_a and δ_r . A scaled $\text{tanh}(\cdot)$ activation function is applied to constrain the actions within the actuator limits. The target critic and actor share the same architectures as their corresponding primary networks.

Remark 2. As the dataset used for off-policy training is collected by an exploration policy, the learned policy may propose actions far from those in the dataset. In such cases, the Q -value estimates can become highly unreliable, leading to inaccurate policy improvement [57]. This problem is especially pronounced when tracking errors change in a large range during training, as the policy has not yet learned to follow the reference. To address this, tracking errors can be clipped to ensure that updates to the critic and actor remain within a safe range, thereby reducing reliance on Out-of-Distribution (OOD) actions [58]. Using $\text{clip}(\cdot)$ prevents large TD errors and Q -value updates caused by excessive tracking errors, which could otherwise destabilize the updates of the critic and actor.

Remark 3. Regularizing the angular rates in the reward design helps reduce overshoot and the amplitude of oscillations during tracking error convergence. This approach is consistent with the rate-feedback control design in the Linear Quadratic Regulator (LQR) [59] and quadratic-cost Approximate Dynamic Programming (ADP) [48], where the rate-weighting parameters in the state-weighting matrix (commonly denoted as Q) are tuned to achieve similar effects.

The training process consists of five independent instances, each initialized with a different random seed. Each instance runs for 3000 episodes. The baseline algorithm adopts DDPG with hyperparameters listed in Table II. The network structures of critic and actor are seen in Figure VIII-A.

TABLE II: RL Algorithm Hyperparameters

Parameter	Value
Critic learning rate η_{critic}	0.001
Actor learning rate η_{actor}	0.001
Delay factor τ	0.01
Discount factor γ	0.99
OU process parameters σ, θ, dt	0.015, 0.1, 0.01
Buffer size	9×10^6
Mini-batch size N	256
Optimizer	Adam
Hidden layer structure	64×64
Critic activation functions	ReLU
Actor output-layer activation function	tanh
Actor hidden-layers activation function	tanh-ReLU
Spatial smoothness loss weight λ_1	3.5×10^{-5}
Temporal smoothness loss weight λ_2	1.11×10^{-5}

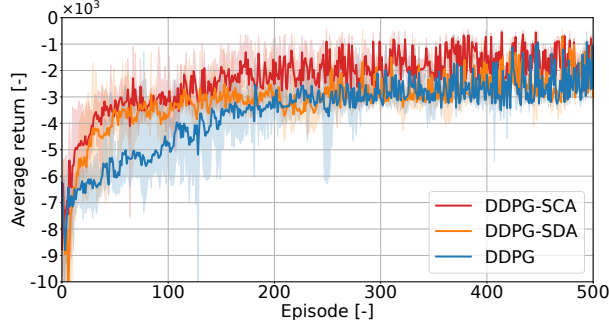


Fig. 6: Online training performance over 500 episodes. The solid line indicates the average return over 5 instances. The dashed line represents the maximum and minimum bounds.

TABLE III: Training performance

Metric/Algorithm	DDPG-SCA	DDPG-SDA	DDPG
Rolling average return at episode 500	-1672.669 ± 250.239	-2408.224 ± 234.935	-2499.168 ± 147.257
Average rate during episodes 1-500	14.212 ± 2.118	8.045 ± 1.058	7.489 ± 2.805
Rolling average return at episode 3000	-1468.781 ± 395.151	-1643.008 ± 345.124	-1654.506 ± 197.981
Average rate during episodes 2500-3000	-0.197 ± 0.678	-0.056 ± 0.212	0.326 ± 0.099

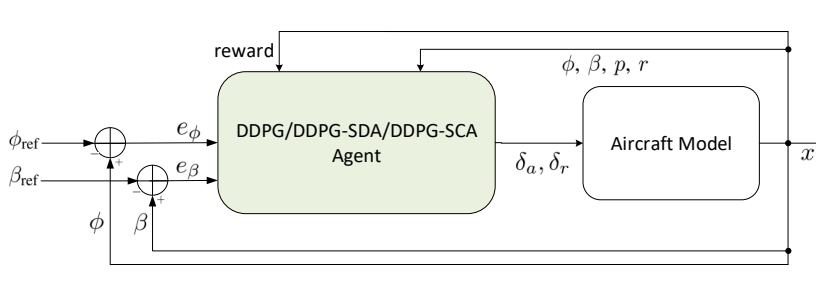


Fig. 4: The architecture of the RL-based flight control system.

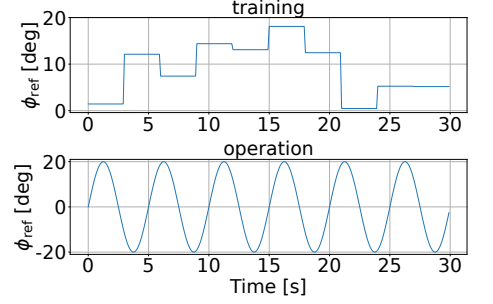


Fig. 5: Bank angle references during training and operation. The training reference varies randomly in amplitude within $[0, 20^\circ]$ with each value held for 3s.

B. Training results

Figure 6 presents the average return over 500 episodes. Symmetry-informed DDPG variants exhibit faster policy convergence than DDPG, owing to the improved sample efficiency provided by symmetric data augmentation. This improvement is particularly evident in the initial phase, when only a limited number of samples are collected using an exploration policy. The second observation lies in that DDPG-SCA improves policy convergence compared to DDPG-SDA, verifying that the augmented samples are utilized more efficiently for training through the two-step approximate value iteration. Furthermore, DDPG-SCA reaches the highest steady-state average return, demonstrating its ability to learn a policy closer to the optimal policy. The average return of DDPG eventually becomes comparable to that of DDPG-SDA after 300 episodes, once the policies have been sufficiently trained. This observation also demonstrates the effectiveness of DDPG's exploration policy.

Figure 7 presents the rolling average return during training over 3000 episodes. The rolling average return is defined as the mean return over the most recent 100 episodes, providing a smoothed performance measure. By episode 3000, all algorithms have settled closely at their sub-optimal values (statistics provided in Table III). The average rate quantifies the rate of change of the rolling average return. Table III shows that the symmetry-informed algorithms exhibit higher average rates than the baseline during the first 500 episodes, enabling accelerated policy convergence. The higher average rate of DDPG-SCA (14.212) compared to DDPG-SDA (8.045) indicates that the two-step approximate value iteration outperforms the one-step method in terms of policy convergence. The low average rates during episodes 2500–3000 confirm that the policies have been sufficiently learned.

C. State-space coverage

Figure 8 shows the state samples used for training in a local state space $S_{\text{local}} = \{[\phi, p, \beta, r]^T \in \mathbb{R}^4 | \phi \in [-30^\circ, 30^\circ], p \in [-150^\circ/\text{s}, 150^\circ/\text{s}], \beta \in [-30^\circ, 30^\circ], r \in [-150^\circ/\text{s}, 150^\circ/\text{s}]\}$. The symmetric distribution of explored and augmented samples

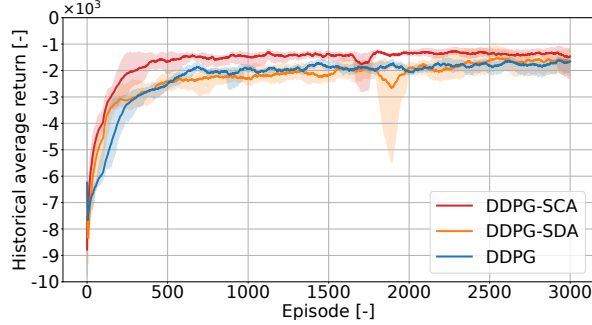


Fig. 7: Online training performance over 3000 episodes. The solid line represents the mean of average returns across five independent runs, while the dashed lines indicate the maximum and minimum values.

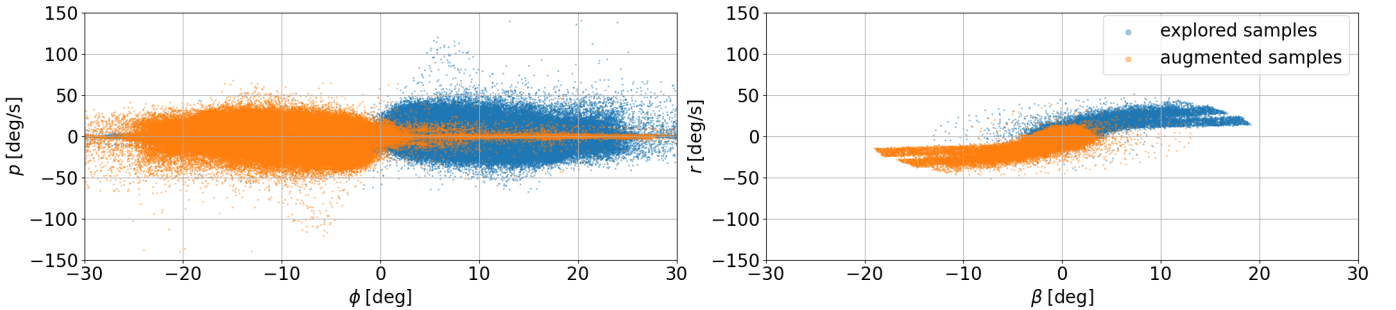


Fig. 8: Distribution of 857,220 training samples in the local state space S_{local} , projected onto two two-dimensional planes.

with respect to the origin reflects the inherent symmetry of the data augmentation process. Explored samples cover only a local region of S_{local} due to the limited capability of the exploration policy. However, the augmented samples compensate for the corresponding symmetric regions that lack exploration, primarily within $[\phi, p, \beta, r] \in [-30^\circ, 0^\circ] \times [-50^\circ/\text{s}, 50^\circ/\text{s}] \times [-20^\circ, 10^\circ] \times [-50^\circ/\text{s}, 0^\circ/\text{s}]$. Discretize S_{local} with a resolution of 1° along the ϕ and β axes, and $10^\circ/\text{s}$ along the p and r axes. The coverage rate is defined as the percentage of four-dimensional unit grids occupied by at least one sample. The explored samples achieve a coverage rate of 16.35%, which increases to 24.09% when augmented samples are included.

D. Attitude tracking

This subsection evaluates the attitude tracking performance under the controllers trained with RL approaches. The reference signals are given as $\phi_{\text{ref}(t)} = 20^\circ \sin(0.2\pi t)$, $\beta_{\text{ref}(t)} = 0$. We assess how the trained agents perform with a bank angle reference that was not used during policy training. A notable characteristic of this bank angle reference is its range across both positive and negative regions, which poses a challenge to the generalization of actors trained only on the positive region provided by the reference during training. During the operation phase, the actor parameters are fixed to the values obtained after 3000 episodes of online training. The initial states are randomized according to the same uniform distributions used during the training phase.

Figures 9 and 10 exhibit the curves of states and actions. It can be observed that the controller trained with DDPG fails to track the bank angle reference in the negative part of bank angle reference, as no samples from this region are collected and used during policy training. Consequently, the controller must produce actions based solely on the neural network's generalization capability. In contrast, the symmetry-informed approaches exhibit comparable tracking performance in the positive and negative parts of the bank angle reference, owing to the additional samples generated by the symmetric data augmentation algorithm.

Subsequently, we evaluate the tracking performance quantitatively in terms of tracking accuracy and control effort. The first metric, Integral of the Absolute Error Mean (IAEM) [60], [61], evaluates tracking error e_t over n trajectories, each with a time horizon $t = 0, 1, \dots, n_e$. It is computed as $\text{IAEM} = \frac{1}{n} \sum_{i=1}^n (\text{IAE})_i$. The auxiliary metric $(\text{IAE})_i = \sum_{t=0}^{n_e} \|e_t^i\|_1 \Delta t$ evaluates the tracking error over a single trajectory indexed by i . Similar to the definition of IAEM, the second metric, the Integral of the Absolute Control Mean (IACM), evaluates the control effort over n trajectories as $\text{IACM} = \frac{1}{n} \sum_{i=1}^n (\text{IAC})_i$, where the auxiliary metric $(\text{IAC})_i = \sum_{t=0}^{n_e} \|u_t^i\|_1 \Delta t$ measures the integral of the absolute control input u_t^i over time $t = 0, 1, \dots, n_e$ for the i -th trajectory. The results are presented in Table IV. A comparison between DDPG-SCA and DDPG-SDA shows that the former achieves more accurate ϕ tracking while requiring less control effort in the roll channel. In contrast, DDPG demonstrates poor tracking performance but better β stabilization compared with the other two approaches.

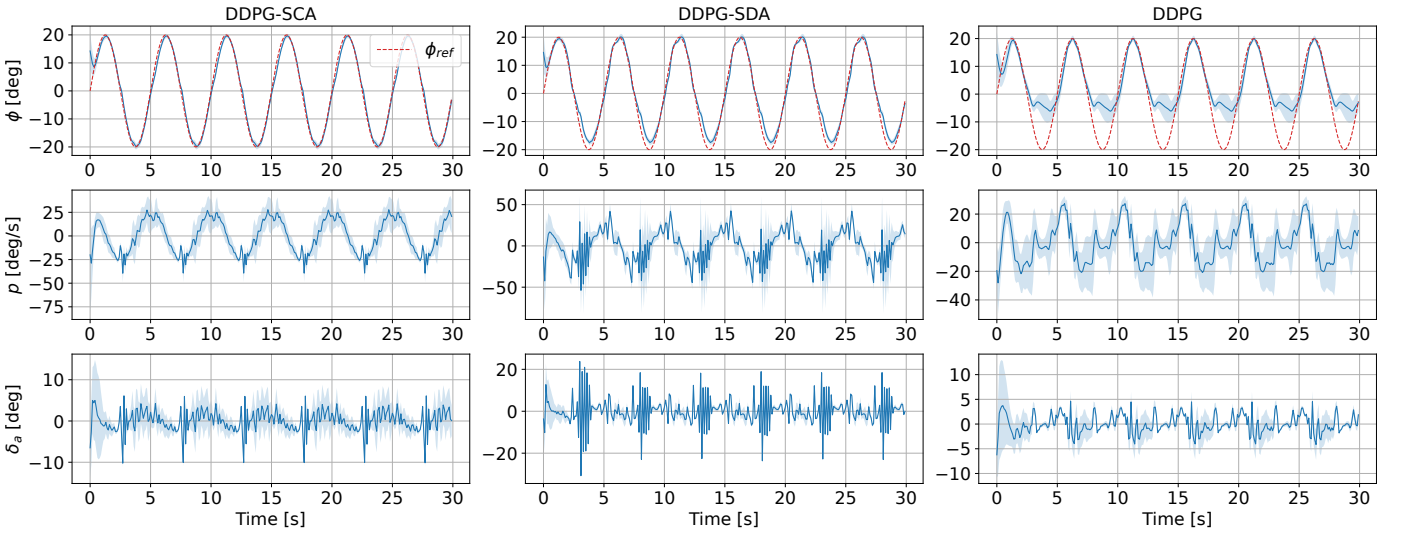


Fig. 9: States and controls in roll channel. The solid lines represent the mean across 5 instances, and the shaded regions indicate one standard deviation.

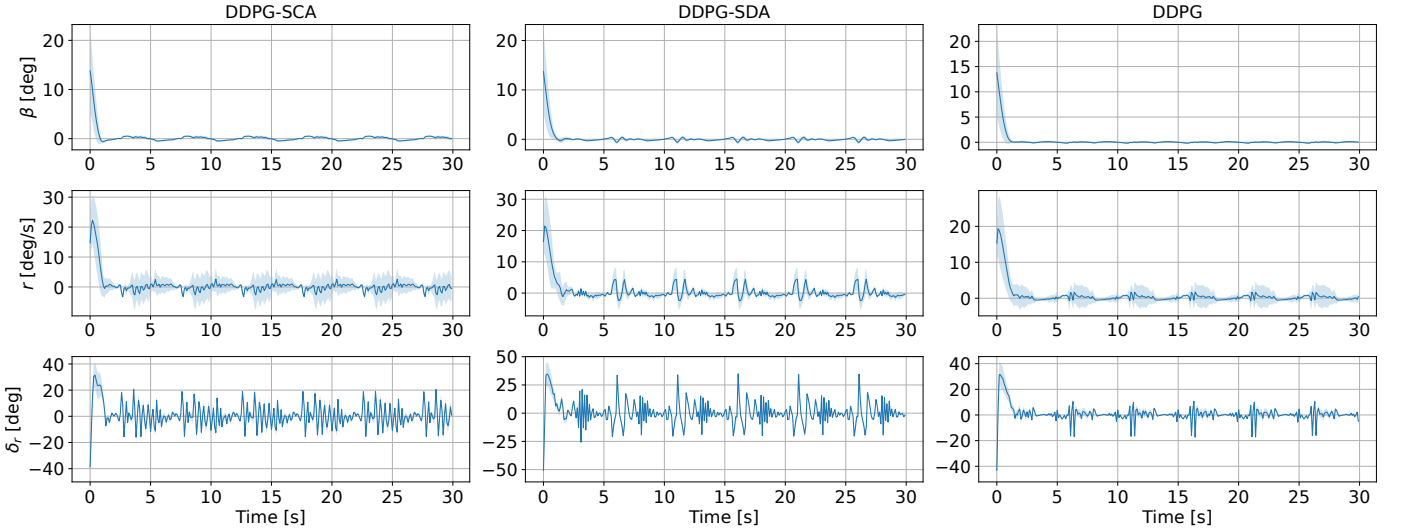


Fig. 10: State and control in yaw channel. The solid lines represent the means across 5 instances, and the shaded regions indicate one standard deviation.

IX. CONCLUSION

This paper has investigated symmetry-informed RL algorithms that exploit the symmetry of dynamical models to generate additional samples. By analyzing the symmetry of the aircraft model, the proposed algorithms demonstrate their suitability for model-free flight control design. Simulation results verify that both DDPG-SCA and DDPG-SDA accelerate convergence toward a suboptimal policy during online training. Moreover, the advantage of the symmetry-informed approaches lies in their ability to ensure control performance in unexplored regions of the state space. This highlights the potential of reducing exploration costs while maintaining controller performance. The benefit stems from the symmetric data augmentation method, which effectively captures symmetric motions in the aircraft dynamics and enables policy learning over an expanded dataset.

TABLE IV: Statistical results of tracking control

Channel	Metric	DDPG-SCA	DDPG-SDA	DDPG
Roll channel	IAEM	1.044	1.136	5.225
	IACM	22.630	26.898	19.649
Yaw channel	IAEM	0.232	0.251	0.212
	IACM	54.466	56.647	50.211

APPENDIX

Proof of Theorem 1

Theorem 2. (Symmetry of x_{t+1}) Select two samples from the system 1, denoted as (x_t, a_t, x_{t+1}) , (x'_t, a'_t, x'_{t+1}) , and a reference state $x = x^*$. Assuming Equations 19, 20 hold, then x_{t+1}, x'_{t+1} are symmetric with respect to x^* when

- (1) $x^* = 0 \in \mathbb{R}^n$, $G(x_t) = G(x'_t)$, $F(x_t) = F(x'_t)$
- (2) $x^* \neq 0 \in \mathbb{R}^n$, $G(x_t) = G(x'_t)$, $F(x_t) = F(x'_t) = I \in \mathbb{R}^{n \times n}$.

Proof. Assume states x_t, x'_t are symmetric to the reference $x = x^*$:

$$\frac{(x_t + x'_t)}{2} = x^* \quad (44)$$

and a_t, a'_t are symmetric to $0 \in \mathbb{R}^n$:

$$a_t = -a'_t \quad (45)$$

The predicted state using the model 1, when taking action a_t at state x_t , is

$$x_{t+1} = F(x_t)x_t + G(x_t)a_t \quad (46)$$

The predicted state using the model 1, when taking action $-a_t$ at state x'_t , is

$$x'_{t+1} = F(x'_t)x'_t - G(x'_t)a_t \quad (47)$$

From 46, 47, one has

$$\begin{aligned} \frac{x_{t+1} + x'_{t+1}}{2} &= \frac{1}{2}[F(x_t)x_t + G(x_t)a_t] + \frac{1}{2}[F(x'_t)x'_t - G(x'_t)a_t] \\ &= \frac{(x_t + x'_t)}{2} + \frac{1}{2}[F(x_t)x_t + G(x_t)a_t - x_t] + \frac{1}{2}[F(x'_t)x'_t - G(x'_t)a_t - x'_t] \end{aligned} \quad (48)$$

Substitute 44 into 48:

$$\begin{aligned} \frac{x_{t+1} + x'_{t+1}}{2} &= x^* + \frac{1}{2}[F(x_t)x_t + G(x_t)a_t - x_t] \\ &\quad + \frac{1}{2}[F(x'_t)x'_t - G(x'_t)a_t - x'_t] \end{aligned} \quad (49)$$

If x_{t+1}, x'_{t+1} are symmetric with respect to x^* , the following equation should hold

$$\frac{x_{t+1} + x'_{t+1}}{2} = x^* \quad (50)$$

Comparing 49 and 50, one has

$$\frac{1}{2}[F(x_t)x_t + G(x_t)a_t - x_t] + \frac{1}{2}[F(x'_t)x'_t - G(x'_t)a_t - x'_t] = 0 \quad (51)$$

Rewrite 51 as

$$\underbrace{\frac{1}{2}[F(x_t) - I]x_t + \frac{1}{2}[F(x'_t) - I]x'_t}_{\text{term1}} + \underbrace{\frac{1}{2}G(x_t)a_t - \frac{1}{2}G(x'_t)a_t}_{\text{term2}} = 0 \quad (52)$$

Equation 52 provides the condition for x_{t+1} and x'_{t+1} to be symmetric with respect to x^* . Terms 1 and 2 describe how the functions $F(x_k)$ and $G(x_k)$ influence the symmetry when x_t and x'_t transition to x_{t+1} and x'_{t+1} . If both term 1 and term 2 are equal to 0, then the symmetry of x_{t+1} and x'_{t+1} is the same as that of x_t and x'_t . If either term 1 or term 2 is nonzero, then x_{t+1} and x'_{t+1} are no longer symmetric.

For further discussion, we consider two cases:

Case 1: $x^* = 0 \in \mathbb{R}^n$, i.e. the reference state is zero.

From 44, one has

$$x_t = -x'_t \quad (53)$$

Substitute 53 into term 1:

$$\begin{aligned} &\frac{1}{2}[F(x_t) - I]x_t + \frac{1}{2}[F(x'_t) - I]x'_t \\ &= \frac{1}{2}[F(x_t) - I]x_t - \frac{1}{2}[F(x'_t) - I]x_t \\ &= \frac{1}{2}[F(x_t) - F(x'_t)]x_t \end{aligned} \quad (54)$$

Because $x_t = 0 \in \mathbb{R}^n$ does not always hold, the condition that term 1 to be identically 0 becomes $F(x_t) = F(x'_t)$.

Rewrite term 2 as

$$\begin{aligned} & \frac{1}{2}G(x_t)a_t - \frac{1}{2}G(x'_t)a_t \\ &= \frac{1}{2}[G(x_t) - G(x'_t)]a_t \end{aligned} \quad (55)$$

Because $a_t = 0$ does not always hold, the condition that term 2 to be identically 0 becomes $G(x_t) = G(x'_t)$.

Case 2: $x^* \neq 0 \in \mathbb{R}^n$, i.e. the reference state is nonzero.

From Equation 44, one has

$$x_t = 2x^* - x'_t \quad (56)$$

Substitute 56 to term 1:

$$\begin{aligned} & \frac{1}{2}[F(x_t) - I]x_t + \frac{1}{2}[F(x'_t) - I]x'_t \\ &= \frac{1}{2}[F(x_t) - I]x_t + \frac{1}{2}[F(x'_t) - I](2x^* - x_t) \\ &= \frac{1}{2}[F(x_t) - I]x_t - \frac{1}{2}[F(x'_t) - I]x_t + [F(x'_t) - I]x^* \\ &= \frac{1}{2}[F(x_t) - F(x'_t)]x_t + [F(x'_t) - I]x^* \end{aligned} \quad (57)$$

Because $x^* \neq 0 \in \mathbb{R}^n$, the condition for 57 equals 0 is

$$\begin{aligned} F(x_t) &= I \\ F(x'_t) &= I \end{aligned} \quad (58)$$

The analysis of term 2 is similar to that in case 1.

Rewrite term 2 as

$$\frac{1}{2}G(x_t)a_t - \frac{1}{2}G(x'_t)a_t = \frac{1}{2}[G(x_t) - G(x'_t)]a_t \quad (59)$$

Because $a_t = 0 \in \mathbb{R}^n$ does not always hold, the condition that term 2 to be identically 0 becomes $G(x_t) = G(x'_t)$. \square

Implementation of two-step approximate value iteration

In this approach, the critics are trained using mini-batches sampled from the replay buffers \mathcal{D}_1 and \mathcal{D}_2 , respectively. The actor is trained twice in each training round by each critic to ensure that both the explored and augmented samples are incorporated into the policy optimization. Target networks are introduced to stabilize the learning process through delayed parameter updates [62].

The *first-step* approximate value iteration is conducted on explored samples. For a mini-batch \mathcal{B}_1 from the replay buffer \mathcal{D}_1 , the Mean Square Error (MSE) loss is calculated as

$$L_{\text{critic}} = \frac{1}{N} \sum_{j=1}^N \delta_j^2 \quad (60)$$

where N is the number of samples in \mathcal{B}_1 , j is the index of samples, δ_j is the Bellman residual on the j th sample:

$$\delta_j = r_t^j + \gamma(\hat{Q}^h)_{\psi_{1\text{target}}}^i(x_{t+1}^j, (\mu_{\theta_{\text{target}}})^i(x_{t+1}^j)) - (\hat{Q}_{\psi_1}^h)^i(x_t^j, a_t^j) \quad (61)$$

where $\psi_{1\text{target}}$ is the parameter set of the target critic.

The gradient of loss L_{critic} with respect to parameter set ψ_1 is derived as

$$\begin{aligned} \frac{\partial L_{\text{critic}}}{\partial \psi_1^i} &= \frac{1}{N} \left(2\delta_1 \frac{\partial \delta_1}{\partial \psi_1^i} + 2\delta_2 \frac{\partial \delta_2}{\partial \psi_1^i} + \cdots + 2\delta_N \frac{\partial \delta_N}{\partial \psi_1^i} \right) \\ &= -\frac{1}{N} \left(2\delta_1 \frac{\partial (\hat{Q}_{\psi_1}^h)^i(x_t^1, a_t^1)}{\partial \psi_1^i} + 2\delta_2 \frac{\partial (\hat{Q}_{\psi_1}^h)^i(x_t^2, a_t^2)}{\partial \psi_1^i} + \cdots + 2\delta_N \frac{\partial (\hat{Q}_{\psi_1}^h)^i(x_t^N, a_t^N)}{\partial \psi_1^i} \right) \\ &= -\frac{2}{N} \sum_{j=1}^N \delta_j \frac{\partial (\hat{Q}_{\psi_1}^h)^i(x_t^j, a_t^j)}{\partial \psi_1^i} \end{aligned} \quad (62)$$

The parameter set ψ_1 is updated as

$$\psi_1^{i+1} = \psi_1^i + \eta_{\text{critic}} \frac{\partial L_{\text{critic}}}{\partial \psi_1^i} \quad (63)$$

The parameter set $\psi_{1\text{target}}$ is updated as

$$\psi_{1\text{target}}^{i+1} = \tau\psi_{1\text{target}}^i + (1 - \tau)\psi_1^{i+1} \quad (64)$$

where $0 < \tau \leq 1$ is a delay factor.

The policy improvement is conducted according to the first critic. The MSE loss of the actor is

$$L_{\text{actor}} = \frac{1}{N} \sum_{j=1}^N l_j \quad (65)$$

where l_j is the estimated state-action value on j th sample.

$$l_j = (\hat{Q}_{\psi_1}^h)^{i+1}(x_t^j, (\mu_\vartheta)^i(x_t^j)) \quad (66)$$

The gradient of loss L_{actor} with respect to actor parameter set ϑ^i is

$$\frac{\partial L_{\text{actor}}}{\partial \vartheta^i} = \frac{1}{N} \left(\frac{\partial l_1}{\partial \vartheta^i} + \frac{\partial l_2}{\partial \vartheta^i} + \cdots + \frac{\partial l_N}{\partial \vartheta^i} \right) \quad (67)$$

where

$$\begin{aligned} \frac{\partial l_j}{\partial \vartheta^i} &= \frac{(\partial \hat{Q}_{\psi_1}^h)^{i+1}(x_t^j, (\mu_\vartheta)^i(x_t^j))}{\partial \vartheta_i} \\ &= \frac{\partial(\hat{Q}_{\psi_1}^h)^{i+1}(x_t^j, (\mu_\vartheta)^i(x_t^j))}{\partial(\mu_\vartheta)^i(x_t^j)} \frac{\partial(\mu_\vartheta)^i(x_t^j)}{\partial \vartheta^i} \end{aligned} \quad (68)$$

The parameter set ϑ is updated once by

$$\vartheta^{i+1} = \vartheta^i + \eta_{\text{actor}} \frac{\partial L_{\text{actor}}}{\partial \vartheta^i} \quad (69)$$

The parameter set $\vartheta_{\text{target}}$ is updated once by

$$\vartheta_{\text{target}}^{i+1} = \tau\vartheta_{\text{target}}^i + (1 - \tau)\vartheta^{i+1} \quad (70)$$

The *second-step* approximate value iteration is conducted on augmented samples. For a mini-batch \mathcal{B}_2 from buffer \mathcal{D}_2 , the MSE loss of the second critic is

$$L_{\text{critic}} = \frac{1}{N} \sum_{j=1}^N \delta_j^2 \quad (71)$$

where N is the number of samples in \mathcal{B}_2 , j is the index of samples, δ_j is the Bellman residual on the j th sample:

$$\delta_j = r_t^j + \gamma(\hat{Q}_{\psi_{2\text{target}}}^h)^i(x_{t+1}^j, (\mu_{\vartheta_{\text{target}}})^{i+1}(x_{t+1}^j)) - (\hat{Q}_{\psi_2}^h)^i(x_t^j, a_t^j) \quad (72)$$

where $\psi_{2\text{target}}$ is the parameter set of the second target critic.

The gradient of loss L_{critic} with respect to the parameter set ψ_2 is

$$\begin{aligned} \frac{\partial L_{\text{critic}}}{\partial \psi_2^i} &= \frac{1}{N} \left(2\delta_1 \frac{\partial \delta_1}{\partial \psi_2^i} + 2\delta_2 \frac{\partial \delta_2}{\partial \psi_2^i} + \cdots + 2\delta_N \frac{\partial \delta_N}{\partial \psi_2^i} \right) \\ &= -\frac{1}{N} \left(2\delta_1 \frac{\partial(\hat{Q}_{\psi_2}^h)^i(x_t^1, a_t^1)}{\partial \psi_2^i} + 2\delta_2 \frac{\partial(\hat{Q}_{\psi_2}^h)^i(x_t^2, a_t^2)}{\partial \psi_2^i} + \right. \\ &\quad \left. \cdots + 2\delta_N \frac{\partial(\hat{Q}_{\psi_2}^h)^i(x_t^N, a_t^N)}{\partial \psi_2^i} \right) \\ &= -\frac{2}{N} \sum_{j=1}^N \delta_j \frac{\partial(\hat{Q}_{\psi_2}^h)^i(x_t^j, a_t^j)}{\partial \psi_2^i} \end{aligned} \quad (73)$$

The actor is updated as

$$\psi_2^{i+1} = \psi_2^i + \eta_{\text{critic}} \frac{\partial L}{\partial \psi_2^i} \quad (74)$$

The target actor is updated as

$$\psi_{2\text{target}}^{i+1} = \tau\psi_{2\text{target}}^i + (1 - \tau)\psi_2^{i+1} \quad (75)$$

The policy improvement is conducted by the second critic. Define the MSE loss as

$$L_{\text{actor}} = \frac{1}{N} \sum_{j=1}^N l_j \quad (76)$$

where l_j is the estimated state-action value on j th sample.

$$l_j = (\hat{Q}_{\psi_2}^h)^{i+1}(x_t^j, (\mu_\vartheta)^{i+1}(x_t^j)) \quad (77)$$

The gradient of loss L_{actor} with respect to parameter set ϑ is derived as

$$\frac{\partial L_{\text{actor}}}{\partial \vartheta^{i+1}} = \frac{1}{N} \left(\frac{\partial l_1}{\partial \vartheta^{i+1}} + \frac{\partial l_2}{\partial \vartheta^{i+1}} + \cdots + \frac{\partial l_N}{\partial \vartheta^{i+1}} \right) \quad (78)$$

where

$$\begin{aligned} \frac{\partial l_j}{\partial \vartheta^{i+1}} &= \frac{\partial (\hat{Q}_{\psi_1}^h)^{i+1}(x_t^j, (\mu_\vartheta)^i(x_t^j))}{\partial \vartheta^{i+1}} \\ &= \frac{\partial (\hat{Q}_{\psi_1}^h)^{i+1}(x_t^j, (\mu_\vartheta)^{i+1}(x_t^j))}{\partial (\mu_\vartheta)^{i+1}(x_t^j)} \frac{\partial (\mu_\vartheta)^{i+1}(x_t^j)}{\partial \vartheta^{i+1}} \end{aligned} \quad (79)$$

The parameter set ϑ is updated for the second time as

$$\vartheta^{i+2} = \vartheta^{i+1} + \eta_{\text{actor}} \frac{\partial L_{\text{actor}}}{\partial \vartheta^{i+1}} \quad (80)$$

The parameter set $\vartheta_{\text{target}}$ is updated for the second time as

$$\vartheta_{\text{target}}^{i+2} = \tau\vartheta_{\text{target}}^{i+1} + (1 - \tau)\vartheta^{i+2} \quad (81)$$

REFERENCES

- [1] P.H. Zipfel, Aerodynamic symmetry of aircraft and guided missiles, *Journal of Aircraft*, vol. 13, no. 7, pp. 470-475, 1976, doi: 10.2514/3.44536.
- [2] Y. Yao, G. Xiong, K. Wang, F. Zhu, F. Wang, Vehicle detection method based on active basis model and symmetry in ITS, *16th International IEEE Conference on Intelligent Transportation Systems (ITSC)*, The Hague, Netherlands, Oct, 2013, doi: 10.1109/ITSC.2013.6728299.
- [3] F. Amadio, A. Colomé, C. Torras, Exploiting symmetries in reinforcement learning of bimanual robotic tasks, *IEEE Robotics and Automation Letters*, vol. 4, no. 2, pp. 1838-1845, 2019, doi: 10.1109/LRA.2019.2898330.
- [4] A. Mahajan, T. Tulabandhula, Symmetry learning for function approximation in reinforcement learning, 2017, arXiv: 1706.02999.
- [5] H. Han, J. Cheng, Z. Xi, B. Yao, Cascade flight control of quadrotors based on deep reinforcement learning, *IEEE Robotics and Automation Letters*, vol. 7, no. 4, pp. 11134-11141, 2022, doi: 10.1109/LRA.2022.3196455.
- [6] J. Huang, W. Zeng, H. Xiong, B. R. Noack, G. Hu and S. Liu, Symmetry-informed reinforcement learning and its application to low-level attitude control of quadrotors, *IEEE Transactions on Artificial Intelligence*, vol 5, no. 3, pp: 1147-1161, 2023, doi: 10.1109/TAI.2023.3249683.
- [7] Y. Wang, J. Sun, H. He, C. Sun, Deterministic policy gradient with integral compensator for robust quadrotor control, *IEEE Transactions on Systems, Man, and Cybernetics: Systems*, vol. 50, no. 10, pp. 3713-3725, 2020, doi: 10.1109/TCYB.2018.2884725.
- [8] B. Ma, Z. Liu, Q. Dang, W. Zhao, J. Wang, Y. Cheng, Deep reinforcement learning of UAV tracking control under wind disturbances environments, *IEEE Transactions on Instrumentation and Measurement*, vol. 72, 2023, doi: 10.1109/TIM.2023.3265741.
- [9] M. Chowdhury, S. Keshmiri, Interchangeable reinforcement-learning flight controller for fixed-wing UASs, *IEEE Transactions on Aerospace and Electronic Systems*, vol. 60, no. 2, pp. 2305-2318, 2024, doi: 10.1109/TAES.2024.3351608.
- [10] E. Bohn, E.M. Coates, D. Reinhardt, T.A. Johansen, Data-efficient deep reinforcement learning for attitude control of fixed-wing UAVs: field experiments, *IEEE Transactions on Neural Networks and Learning Systems*, vol. 35, no. 3, pp. 3168-3180, 2024, doi: 10.1109/TNNLS.2023.3263430.
- [11] H. Jiang, H. Xiong, W. Zeng and Y. Ou, Safely learn to fly aircraft from human: an offline-online reinforcement learning strategy and its application to aircraft stall recovery, *IEEE Transactions on Aerospace and Electronic Systems*, vol. 59, no. 6, pp: 8194-8207, 2023, doi: 10.1109/TAES.2023.3299913.
- [12] B. Ma, Z. Liu, W. Zhao, J. Yuan, H. Long and X. Wang, Target tracking control of UAV through deep reinforcement learning, *IEEE Transactions on Intelligent Transportation Systems*, vol. 24, no. 6, pp. 5983-6000, 2023, doi: 10.1109/TITS.2023.3249900.
- [13] R.S. Sutton, A.G. Barto, Reinforcement Learning: An Introduction, *Sigma Series in Pure Mathematics*, Cambridge, MA, USA: A Bradford Book, 2018, ISBN: 978-0262039246.
- [14] S. Mishra, A. Abdolmaleki, A. Guez, P. Trochim, D. Precup, Augmenting learning using symmetry in a biologically-inspired domain, arXiv: 1910.00528
- [15] G. Angelotti, N. Drougard, C.P.C. Chanel, Expert-guided symmetry detection in Markov decision process, *Proceedings of the 14th International Conference on Agents and Artificial Intelligence (ICAART)*, vol. 2, pp. 88-98, 2022, doi: 10.5220/0010783400003116.
- [16] G. Angelotti, N. Drougard, C.P.C. Chanel, Data augmentation through expert-guided symmetry detection to improve performance in offline reinforcement learning, *15th International Conference on Agents and Artificial Intelligence*, Lisbon, Portugal, 2023, doi: 10.5220/0011633400003393.
- [17] J. Brandstetter, M. Welling, D.E. Worral, Lie point symmetry data augmentation for neural PDE solvers, *Proceedings of the 39th International Conference on Machine Learning (ICML)*, Baltimore, Maryland, USA, 2022, url: <https://proceedings.mlr.press/v162/brandstetter22a/brandstetter22a.pdf>.
- [18] R. Wang, R. Walters, and R. Yu, Incorporating symmetry into deep dynamics models for improved generalization, *International Conference on Learning Representations (ICLR)*, Virtual only conference, 2021, url: https://openreview.net/pdf?id=wta_8Hx2KD.
- [19] R. Wang, R. Walters, R. Yu, Data augmentation vs. equivariant networks: a theory of generalization on dynamics forecasting, *Proceedings of the 39th International Conference on Machine Learning (ICML)*, Baltimore, Maryland USA, 2022, doi: arXiv.2206.09450.

[20] Y. Lin, J. Huang, M. Zimmer, J. Rojas, P. Weng, Towards more sample efficiency in reinforcement learning with data augmentation, *NeurIPS Workshop on "Robot Learning: Control and Interaction in the Real World"*, Vancouver, Canada, 2019, url: <http://www.robot-learning.ml/2019/files/papers/Towards%20More%20Sample%20Efficiency%20in%20Reinforcement%20Learning%20with%20Data%20Augmentation.pdf>.

[21] Y. Lin, J. Huang, M. Zimmer, Y. Guan, J. Rojas, P. Weng, Invariant transform experience replay: data augmentation for deep reinforcement learning, *IEEE Transactions on Robotics and Automation Letters*, vol. 5, no. 4, pp: 6615-6622, 2020, doi: 10.1109/LRA.2020.3013937.

[22] C. Pinneri, S. Bechtle, M. Wulfmeier, A. Byravan, J. Zhang, W. F. Whitney, M. A. Riedmiller, Equivariant data augmentation for generalization in offline reinforcement learning, *arXiv preprint*, 2023, doi: 10.48550/arXiv.2309.07578.

[23] T.P. Lillicrap, J.J. Hunt, A. Pritzel, N. Heess, T. Erez, Y. Tassa, D. Silver, D. Wierstra, Continuous control with deep reinforcement learning, *4th International Conference on Learning Representations (ICLR)*, San Juan, Puerto Rico, 2016, doi: arXiv.1509.02971.

[24] M. Weissenbacher, S. Sinha, A. Garg, Y. Kawahara, Koopman Q-learning: offline reinforcement learning via symmetries of dynamics, *Proceedings of the 39th International Conference on Machine Learning (ICML)*, Baltimore, Maryland, USA, 2022, url: <https://proceedings.mlr.press/v162/weissenbacher22a/weissenbacher22a.pdf>.

[25] P. Razzaghi, A. Tabrizian, W. Guo, S. Chen, A. Taye, E. Thompson, A. Bregeon, A. Baheri, P. Wei, A survey on reinforcement learning in aviation applications, *Engineering Applications of Artificial Intelligence*, Vol. 136, pp. 108919, 2024, doi: 10.1016/j.engappai.2024.108911.

[26] D. J. Richter, R. A. Calix and K. Kim, A review of reinforcement learning for fixed-wing aircraft control tasks, *IEEE Access*, vol. 13, 2025, doi: 10.1109/ACCESS.2024.3433540.

[27] W. Völker, Y. Li, E. van Kampen, Twin-delayed deep deterministic policy gradient for altitude control of a flying-wing aircraft with an uncertain aerodynamic model, *AIAA SciTech*, 19 January, 2023, doi: 10.2514/6.2023-2678.

[28] V. Gavra, E. van Kampen, Evolutionary reinforcement learning: hybrid approach for safety-informed fault-tolerant flight control, *Journal of Guidance, Control and Dynamics*, vol.47, no.5, pp. 887-900, 2024, doi: 10.2514/1.G008112.

[29] W. Hu, Y. Yang, Z. Liu, Deep deterministic policy gradient agent-based sliding mode control for quadrotor attitudes, *Drones*, vol. 8, no. 3, 2024, doi: 10.3390/drones8030095.

[30] A. Liu, L. Liu, J. Cao and F. E. Alsaadi, Deep deterministic policy gradient with generalized integral compensator for height control of quadrotor, *Journal of Applied Analysis & Computation*, vol. 12, no. 3, 2022, doi: 10.11948/20210442.

[31] H. Liu, S. Suzuki, W. Wang, H. Liu and Q. Wang, Robust control strategy for quadrotor drone using reference model-based deep deterministic policy gradient, *Drones*, vol. 6, no. 9, 2022, doi: 10.3390/drones6090251.

[32] S. Mysore, B. Mabsout, R. Mancuso and K. Saenko, Regularizing action policies for smooth control with reinforcement learning, *2021 IEEE International Conference on Robotics and Automation (ICRA)*, Xi'an, China, 2021, url: arXiv:2012.06644.

[33] K. Li, W. Ni, Y. Emami and F. Dressler, Data-driven flight control of internet-of-drones for sensor data aggregation using multi-agent deep reinforcement learning, *IEEE Wireless Communications*, vol.29, no.4, pp. 18-23, 2022, doi: 10.1109/MWC.002.2100681.

[34] Y. Liu and C. Huang, DDPG-based adaptive robust tracking control for aerial manipulators with decoupling approach, *IEEE Transactions on Cybernetics*, vol.52, no.8, pp. 8582-8271, 2022, doi: 10.1109/TCYB.2021.3049555.

[35] S. Chen, J. Xiao and C.Y. Hu, A control method for quadrotor based on DDPG, *Advances in Guidance, Navigation and Control*, pp. 5359-5371, 2022, doi: 10.1007/978-981-15-8155-7-442.

[36] A. De Marco, P. M. D'Onza, S. Manfredi, A deep reinforcement learning control approach for high-performance aircraft, *Nonlinear Dynamics*, Vol. 111, pp. 17037-17077, 2023, doi: 10.1007/s11071-023-08725-y.

[37] D.H. Budiarti, Development of model free flight control system using Deep Deterministic Policy Gradient (DDPG), *PhD Thesis*, Cranfield University, 2019, url: <https://dspace.lib.cranfield.ac.uk/handle/1826/20268>.

[38] J. Tang, N. Xie, K. Li, Y. Liang and X. Shen, Trajectory tracking control for fixed-wing UAV based on DDPG, *Journal of Aerospace Engineering*, vol.37, no.3, 2024, url: 10.1061/IAEEEZ.ASENG-5286.

[39] K. Xu, S. Tian and J. Xia, Investigation of deep reinforcement learning for longitudinal-axis flight control, *Journal of Aerospace Engineering*, vol.37, no.2, 2022, doi: 10.1061/IAEEEZ.ASENG-5007.

[40] Y. Li, E. van Kampen, Reinforcement learning-based intelligent flight control for a fixed-wing aircraft to cross an obstacle wall, *European Control Conference (ECC)*, Stockholm, 2024, doi: 10.23919/ECC64448.2024.10591030.

[41] R. Guo, Z. Yao, Z. Kan, D. Li, A disturbance rejection control method for carrier landing based on DDPG algorithm, *IEEE Transactions on Aerospace and Electronic Systems*, pp. 1-18, 2025, doi: 10.1109/TAES.2025.3610815.

[42] D. Shukla, H. Benyamin, S. Keshmiri and N. M. Beckage, Reinforcement learning-based evolving flight controller for fixed-wing uncrewed aircraft, *IEEE Transactions on Control Systems Technology*, vol.33, no.3, pp. 872-886, 2024, doi: 10.1109/TCST.2024.3516383.

[43] D. Sufiyan, L. T. S. Win, S. K. Win, G.S. Soh and S. Foong, A reinforcement learning approach for control of a nature-inspired aerial vehicle, *International Conference on Robotics and Automation (ICRA)*, Montreal, Canada, 24 May, 2019, doi: 10.1109/ICRA.2019.8794446.

[44] Y. Song, Z. Liu, J. Han, J. Yuan, W. Zhao, Q. Dang, Second-order sliding mode control of flying-wing aircraft based on feedforward neural networks, *IEEE Transactions on Automation Science and Engineering*, vol. 22, pp. 21811-21830, 2025, doi: 10.1109/TASE.2025.3613383.

[45] X. Song, J. Duan, W. Wang, S. E. Li, C. Chen, B. Cheng, B. Zhang, J. Wei, X.S. Wang, LipsNet: a smooth and robust neural network with adaptive Lipschitz constant for high accuracy optimal control, *32nd Conference on Neural Information Processing Systems (NeurIPS)*, Montréal, Canada, 2018, url: https://proceedings.neurips.cc/paper_files/paper/2018/file/d54e99a6c03704e95e6965532dec148b-Paper.pdf.

[46] T. Avant, K.A. Morgansen, Analytical bounds on the local Lipschitz constants of ReLU networks, *IEEE Transactions on Neural Networks and Learning Systems*, vol. 35, no. 10, pp. 13902-13913, 2024, doi: 10.48550/arXiv.2104.14672.

[47] K. Scaman and A. Virmaux, Lipschitz regularity of deep neural networks: analysis and efficient estimation, *32nd Conference on Neural Information Processing Systems (NeurIPS 2018)*, Montreal, Canada, 2018, url: https://proceedings.neurips.cc/paper_files/paper/2018/file/d54e99a6c03704e95e6965532dec148b-Paper.pdf.

[48] A. Heydari, Theoretical and numerical analysis of approximate dynamic programming with approximation errors, *Journal of Guidance, Control, and Dynamics*, vol. 39, no. 2, pp. 301-311, 2016, doi: 10.2514/1.G001154.

[49] J. Obando-Ceron, M. G. Bellemare, P.S. Castro, Small batch deep reinforcement learning, *37th Conference on Neural Information Processing Systems (NeurIPS)*, New Orleans, USA, 2023, url: https://proceedings.neurips.cc/paper_files/paper/2023/file/528388f1ad3a481249a97cbb698d2fe6-Paper-Conference.pdf.

[50] J.L. Doob, The Brownian movement and stochastic equations, *Annals of Mathematics*, vol. 43, no. 2, pp. 351-369, 1942, doi: 10.2307/1968873.

[51] H. Ohta, P.N. Nikiforuk and M.M. Gupta, Design of desirable handling qualities for aircraft lateral dynamics, *Journal of Guidance, Control and Dynamics*, vol.2, no.1, pp. 31-39, 1979, doi: 10.2514/3.55828.

[52] H.J. Stetter, *Analysis of Discretization Methods for Ordinary Differential Equations*, Society for Industrial and Applied Mathematics(SIAM), Philadelphia, USA: 1973, doi: 10.1137/1016100.

[53] K. Dally, E. van Kampen, Soft actor-critic deep reinforcement learning for fault tolerant flight control, *AIAA Scitech 2022 Forum*, San Diego, CA & Virtual, USA, 2020, doi: 10.2514/6.2022-2078.

[54] L. Vieira dos Santos and E. van Kampen, Safe & smart control: hybrid and distributional reinforcement learning for attitude flight control, *AIAA Scitech 2025 Forum*, Orlando, FL, USA, 2025, doi: 10.2514/6.2022-2078.

[55] M. Homola, E. van Kampen, Uncertainty-driven distributional reinforcement learning for flight control, *AIAA Scitech 2025 Forum*, Orlando, FL, USA, 2025, doi: 10.2514/6.2025-2793.

- [56] K. He, X. Zhang, S. Ren, J. Sun, Delving deep into rectifiers: surpassing human-level performance on ImageNet classification, *IEEE International Conference on Computer Vision (ICCV)*, 18 February, 2015, doi: 10.1109/ICCV.2015.123.
- [57] H. P. van Hasselt, Double Q -learning, *Advances in Neural Information Processing Systems*, December 2010, The MIT Press, url: https://proceedings.neurips.cc/paper_091d584fc301b442654dd8c23b3fc9-Paper.pdf.
- [58] G. An, S. Moon, J. Kim, H.O. Song, Uncertainty-based offline reinforcement learning with diversified Q -ensemble, *Advances in Neural Information Processing Systems*, December 2021, The MIT Press, <https://proceedings.neurips.cc/paper/2021/file/3d3d286a8d153a4a58156d0e02d8570c-Paper.pdf>.
- [59] F.L. Lewis, D. Vrabie and V.L. Syrmos, *Optimal Control*, Wiley, 3rd edition, 2012, ISBN: 978-0-470-63349-6.
- [60] S.M. Shinmer, Modern control system theory and application, 2nd ed., Addison-Wesley, Illinois, USA: 1978, [Online], Available: <https://www.wiley.com/en-us/Modern+Control+System+Theory+and+Design%2C+2nd+Edition-p-9780471249061>.
- [61] Z. Guo, J. Zhou, G. Guo, J. Cieslak, J. Chang, Coupling characterization-based robust attitude control scheme for hypersonic vehicles, *IEEE Transactions on Industrial Electronics*, vol.64, no. 8, 2017, doi: 10.1109/TIE.2017.2682031.
- [62] S. Zhang, H. Yao, S. Whiteson, Breaking the deadly triad with a target network, *Proceedings of the 38th International Conference on Machine Learning (ICML)*, 2021, url: https://proceedings.mlr.press/v139/zhang21y/zhang21y.pdf?utm_source=chatgpt.com.



Yifei Li (Graduate Student Member, IEEE) received the B.Sc. and M.Sc. degrees from Northwestern Polytechnical University, Xi'an, China, in 2017 and 2020, respectively. He is currently pursuing the Ph.D. degree with the Section Control and Simulation, Delft University of Technology, Delft, The Netherlands. His research interests include reinforcement learning, aerospace control.



Erik-Jan van Kampen received the B.Sc. degree in aerospace engineering, the M.Sc. degree in control and simulation, and Ph.D. degree in aerospace engineering from the Delft University of Technology, Delft, the Netherlands, in 2004, 2006, and 2010, respectively. He is currently an Associate Professor with the Control and Simulation Division, Delft University of Technology. His current research interests include intelligent flight control, adaptive control, and interval optimization.